Journal of Catalysis 278 (2011) 276–287

Contents lists available at ScienceDirect

Journal of Catalysis

journal homepage: www.elsevier.com/locate/jcat

Silver nanoparticles supported on TiO_2 nanotubes as active catalysts for ethanol oxidation

Y.Q. Liang [a], Z.D. Cui [a], S.L. Zhu [a,b], Y. Liu [a], X.J. Yang [a,b,*]

[a] School of Materials Science and Engineering, Tianjin University, Tianjin 300072, China
[b] Tianjin Key Laboratory of Composite and Functional Materials, Tianjin 300072, China

ARTICLE INFO

Article history:
Received 13 October 2010
Revised 15 December 2010
Accepted 17 December 2010
Available online 3 February 2011

Keywords:
Ethanol oxidation
TiO_2 nanotubes
Ag nanoparticles
Polyol process

ABSTRACT

Silver (Ag) nanoparticles were successfully assembled in self-organized TiO_2 nanotubes by the polyol process. Scanning electron microscopy, transmission electron microscopy, X-ray diffraction, X-ray photoelectron spectroscopy as well as Fourier transform infrared spectroscopy were used for the characterization of surface morphology, phase composition, microstructure, and valent state of the Ag—TiO_2 catalysts. It was found that these catalysts showed improved dispersion and increased catalytically active sites. The electrocatalytic properties of Ag—TiO_2 catalysts for ethanol oxidation were investigated by cyclic voltammetry. The results showed that the Ag doped anatase TiO_2 composites exhibited excellent catalytic activity in electrocatalytic ethanol oxidation in alkaline media. Hence, the composites look promising in direct ethanol fuel cell applications.

1. Introduction

With the energy shortage becoming more and more serious, people are looking for environmentally friendly transportation fuels to replace conventional fossil fuels. At present, considerable research is focused on the development of high surface area electrocatalysts, which has high catalytic activity for methanol oxidation and resistance to catalyst poisoning [1]. In the past decades, ethanol has received increased attention because it has fuel characteristics similar to those of methanol. However, from an energy storage point of view, ethanol appears to be a preferable fuel over methanol. Also, ethanol is much less toxic and expensive than methanol; thus, the threat to the environment can be dramatically attenuated [2]. For these reasons, ethanol was adopted to evaluate the catalytic activity in this study. Nanosized TiO_2, one of the most popular catalyst materials, has the advantages of physical and chemical stability, high activity, and low price. Among various TiO_2 morphologies, TiO_2 nanotubes are attractive substrates because of their large specific surface areas, thermal stability, chemical inertness, and nontoxicity [3]. In addition, noble metal catalysts also attract considerable attention due to their unique nature. Therefore, metals such as Au, Pt, Rh, and Pd deposited on the surface of TiO_2 have shown excellent performance in the activity and stability [4–7]. However, these noble metals are too expensive to use at an industrial scale. Recently, silver doped TiO_2 (Ag—TiO_2) nanocomposite structures have attracted much attention not only because TiO_2 is a promising material with desirable electronic and optical properties, but also because Ag displays some unique activities in chemical and biological sensing compared with the other noble metals mentioned above [8]. Thus, the study of Ag modified TiO_2 has significant practical value. To date, it has been shown in many reports that impregnating TiO_2 with noble metals, such as Pd, Au, or Pt could effectively improve the photocatalytic activity of TiO_2 [9,10]. However, the electrocatalytic activity of Ag doped TiO_2 nanotubes has not been subjected to intensive study. It is well known that TiO_2 has three crystal phases (anatase, rutile, and brookite). However, the influence of TiO_2 crystal phase on the electrocatalytic activity has not been reported in detail.

The photoreduction method was usually employed to synthesize Ag doped TiO_2 nanotube composites [11]. It was observed that photoreduced Ag cannot be highly dispersed on the surface of TiO_2. Hence, the amount of active sites on the Ag—TiO_2 surface cannot be increased significantly. Other methods involving sol–gel, 'wet' chemical and ceramic methods, where drying, heating or annealing at high temperatures are important steps in the preparation process [12–14], are too complicated for large-scale production. It is well known that the polyol process is a convenient, versatile and low-cost method for the synthesis of metal nanostructures on a large scale. Based on this technique, a number of metal nanostructures, such as gold nano-octahedra [15], gold nanoplates [16], Ag nanowires [17] and Ag nanopowder [18], have been successfully synthesized in ethylene glycol (EG) solution.

* Corresponding author at: School of Materials Science and Engineering, Tianjin University, Tianjin 300072, China.
E-mail address: xjyang@tju.edu.cn (X.J. Yang).

0021-9517/$ - see front matter © 2010 Elsevier Inc. All rights reserved.
doi:10.1016/j.jcat.2010.12.011

In order to modify the TiO_2 nanotubes by Ag nanoparticles, a polyol method at low-temperature has been developed to overcome the difficulties and disadvantages mentioned above. The Ag^+ ions from silver nitrate ($AgNO_3$) can be reduced to metallic Ag, some of which can be deposited onto the nanotube surface, while the others may react with the small amount of ruitle TiO_2 to form the silver titanate. We have found no study on the preparation of simultaneously doped and deposited Ag on TiO_2 nanotubes using this method.

In order to prepare Ag—TiO_2 composite nano-material, a small amount of sodium borohydride ($NaBH_4$) was added to an EG solution of polyvinylpyrrolidone (PVP) prior to the addition of $AgNO_3$ aqueous solution. In this process, the $AgNO_3$ solution serves as the metal salt precursor, $NaBH_4$ as the reductant, and EG as both a solvent for the precursors and a reductant for the reaction. Previous studies revealed that the surfactant PVP could act not only as a stabilizer to prevent the aggregation of the products but also as a shape controller to assist the formation of anisotropic metal nanostructures. The advantage of this method is that the EG can serve not only as solvent but also as reducing reagent. The use of EG may lead to a more environment-friendly production of Ag nanoparticles deposited on TiO_2 surfaces as well as to an increase in stability of the obtained Ag—TiO_2 colloids [19]. In this study, the Ag nanoparticles were deposited successfully on different crystal phases of TiO_2. Furthermore, the electrocatalytic activity of the Ag—TiO_2 catalysts was also evaluated.

2. Experimental

2.1. Synthesis of self-organized TiO_2 nanotube arrays on Ti substrate

TiO_2 nanotubes on Ti substrates were fabricated by anodic oxidation according to a method reported in the literature [20]. Briefly, commercial pure titanium sheets (11 mm × 9 mm × 0.6 mm, Tianjin Pengbo Company, China) were used as the substrate electrode. Prior to anodic oxidation, the titanium sheets were ground with different types of emery paper (600#, 1000#, and 2000#) and then degreased in an ultrasonic bath in ethanol and deionized (DI) water followed by air drying. Samples were anodized in water/glycerol (1:1 Vol.%) mixtures containing 0.3 M NH_4F at a potential of 30 V for 3 h. Finally, the as-prepared TiO_2 nanotube electrode was annealed at 723 and 923 K under oxygen atmosphere for 1 h.

2.2. Chemical assembly of Ag nanoparticles in TiO_2 nanotubes

PVP was added to water/ EG (1:1 Vol.%) mixtures in a beaker. The mixture was stirred for about 5 min, and then, $NaBH_4$ was introduced under stirring. After 1–2 min, $AgNO_3$ was added. These operations were performed at room temperature. The solution appeared deep brown owing to the presence of Ag^+ ions. The concentrations of Ag^+ ions, $NaBH_4$ and PVP were about 0.035, 0.026, and 0.001 M, respectively. All reagents were analytical grade. The as-prepared TiO_2 nanotube sample was immersed in this electrolyte under static conditions at 40 °C for 3, 7, and 11 h, and subsequently rinsed with DI water and air dried. The surface morphology and structure of samples were characterized by field emission scanning electron microscopy (FE-SEM, Hitachi S-4800), X-ray diffraction (XRD, RIGAKU/DMAX), and transmission electron microscopy (TEM, Philips Tecnai G2 F20). Surface chemical analysis of Ag—TiO_2 coatings were performed by X-ray photoelectron spectroscopy (XPS) using a PHL1600ESCA instrument equipped with a monochromatic Mg Ka X-ray source (E = 1253.6 eV) source operated at 250 W. The analysis spot had a diameter of 200 μm, and the detection angle relative to the substrate surface was 45°. In such conditions, the probed depth was estimated to be around 3 nm. Peak position was internally referenced to the C1s peak at 284.5 eV. Fourier transform IR Spectra (FTIR) of Ag—TiO_2 coatings were measured by Fourier transform IR Spectrometer (WQF-510) to study the chemical interactions between PVP molecules and $AgNO_3$ as well as the composition evolution during the Ag formation processes. The obtained Ag—TiO_2 coatings were first removed from the titanium substrate and dried under vacuum in a desiccator prior to the FTIR analysis. Then, the samples were grinded into fine powder, which involves mixing thoroughly the material to be tested with KBr before forming a pellet at high pressure.

2.3. Characterization of electrocatalytic properties of Ag—TiO_2 nanotubes

The effect of ethanol on the catalytic activities of the catalysts was determined by cyclic voltammetry (CV) in acidic medium containing C_2H_5OH (0.5 M)—H_2SO_4 (0.1 M) and alkaline medium containing C_2H_5OH (0.5 M)—NaOH (0.1 M). All the electrochemical measurements were performed on an electrochemical workstation (Gamry Reference 600, Gamry, USA). The electrochemical measurements were carried out with a conventional three-electrode system. The Ag—TiO_2 nanotube electrode was used as the working electrode, a platinum electrode as the counter electrode and a saturated calomel electrode (SCE) as the reference electrode in all cases.

3. Results and discussion

Fig. 1 shows the SEM images of the as-formed TiO_2 nanotubes (a, b), Ag-fresh TiO_2 (c, d), Ag—TiO_2/723 K (e, f), and Ag—TiO_2/923 K (g, h) coatings in the top, bottom and cross-sectional views after 7 h deposition. The morphology of the synthesized TiO_2 nanotubes is shown in Fig. 1a and b. The nanotubes (with diameter of 120 nm and length of 1.2 μm) are vertically aligned on the Ti substrate by anodization. The bottoms of the tubes have a flute-shape structure. It is apparent from Fig. 1c the ordered and evenly distributed Ag nanoparticles with average diameter of 20 nm are formed preferentially on the exterior mouth of the amorphous TiO_2 nanotubes. After the nanotubes were annealed at 723 K, the Ag nanoparticles were deposited on them under the same method (see Fig. 1e). Some Ag nanoparticles were dispersed on the pore openings and showed a distribution less dense than that in Fig. 1c, while some were deposited into the nanotubes, as indicated by the arrows. It can be presumed that the nanotubes annealed at 723 K facilitate the Ag formation on the tube surface, leading to high electrocatalytic activity as discussed later. However, the nanotubes annealed at 923 K seem to exhibit unfavorable properties for depositing ordered Ag nanoparticles, as shown in Fig. 1g. It is obvious that some particle aggregates are located on the tube surface, while some were not formed completely. This result may be due to the incomplete reaction of $AgNO_3$, which will be further confirmed by XPS results in a later section. Meanwhile, images of the bottom and cross-section of the Ag doped samples are also shown in Fig. 1d, f and h. According to the SEM image of the bottom shown in Fig. 1d, the space between two nanotubes is filled by Ag nanoparticles. Also, the Ag nanoparticles can permeate into the flutes of tube bottoms by passing through their interstices. Apparently, the boundary between the Ag nanoparticles and the nanotubes disappear and become gradually integrated after annealing at 723 K, as shown in Fig. 1f. In addition, the cross-sectional image in Fig. 1f shows that the sidewall of the nanotubes was almost entirely covered by Ag nanoparticles. But the inset in Fig. 1d shows that Ag nanoparticles mainly adhere to the upper

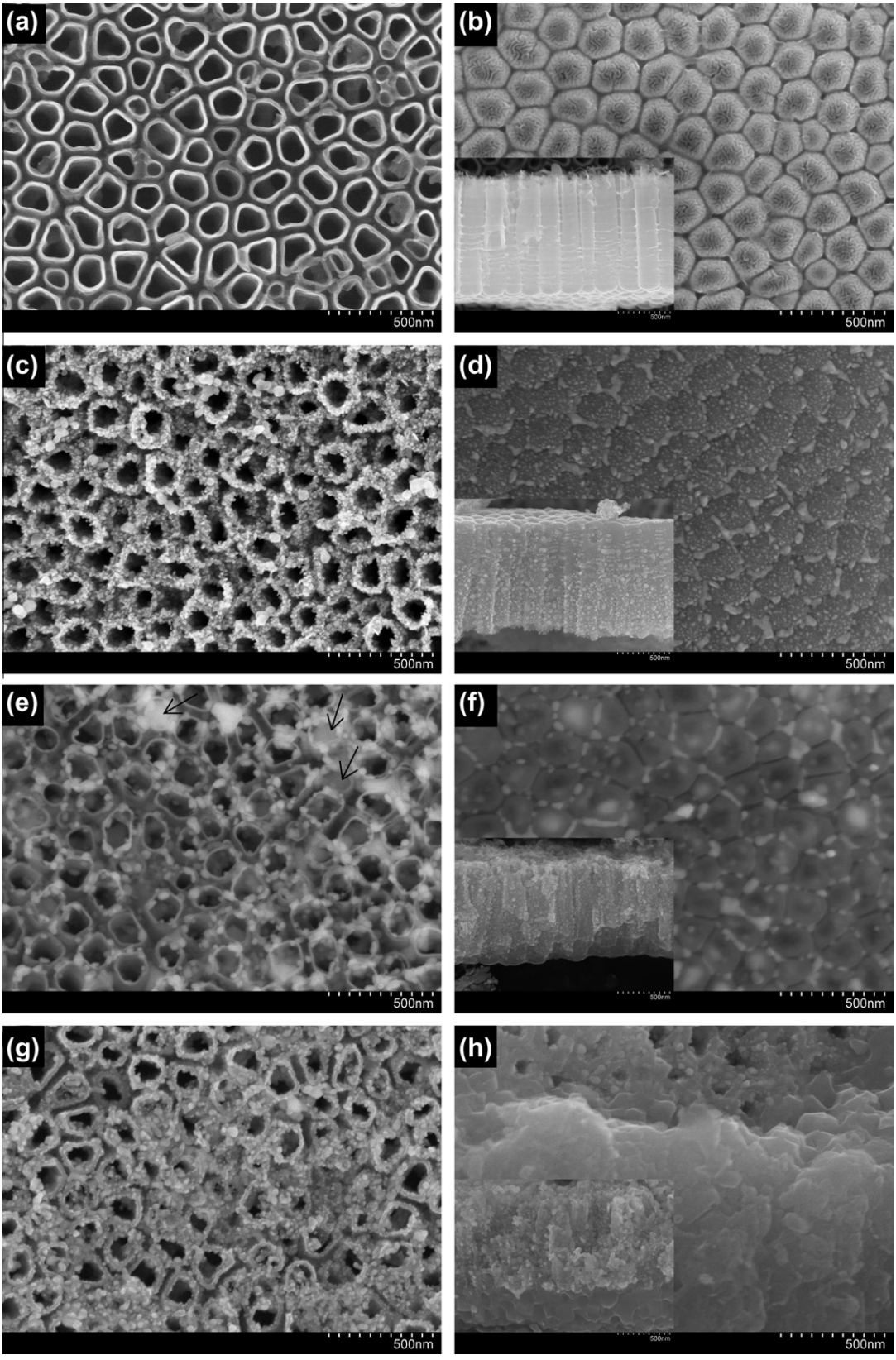

Fig. 1. SEM top and bottom images of as-formed TiO_2 nanotubes (a) and (b), Ag doped fresh TiO_2 nanotubes (c) and (d), Ag doped TiO_2 nanotubes annealed at 723 K (e) and (f), Ag doped TiO_2 nanotubes annealed at 923 K (g) and (h). The insets show the cross-sectional view of corresponding samples.

part of the tube wall. Unfortunately, the nanotube structures were destroyed as shown in the bottom and cross-sectional images in Fig. 1h. The destruction can be ascribed to the high-temperature annealing at 923 K. The irregular nanotubes and the rutile structure (obtained by annealing at 923 K) may retard the formation of Ag nanoparticles.

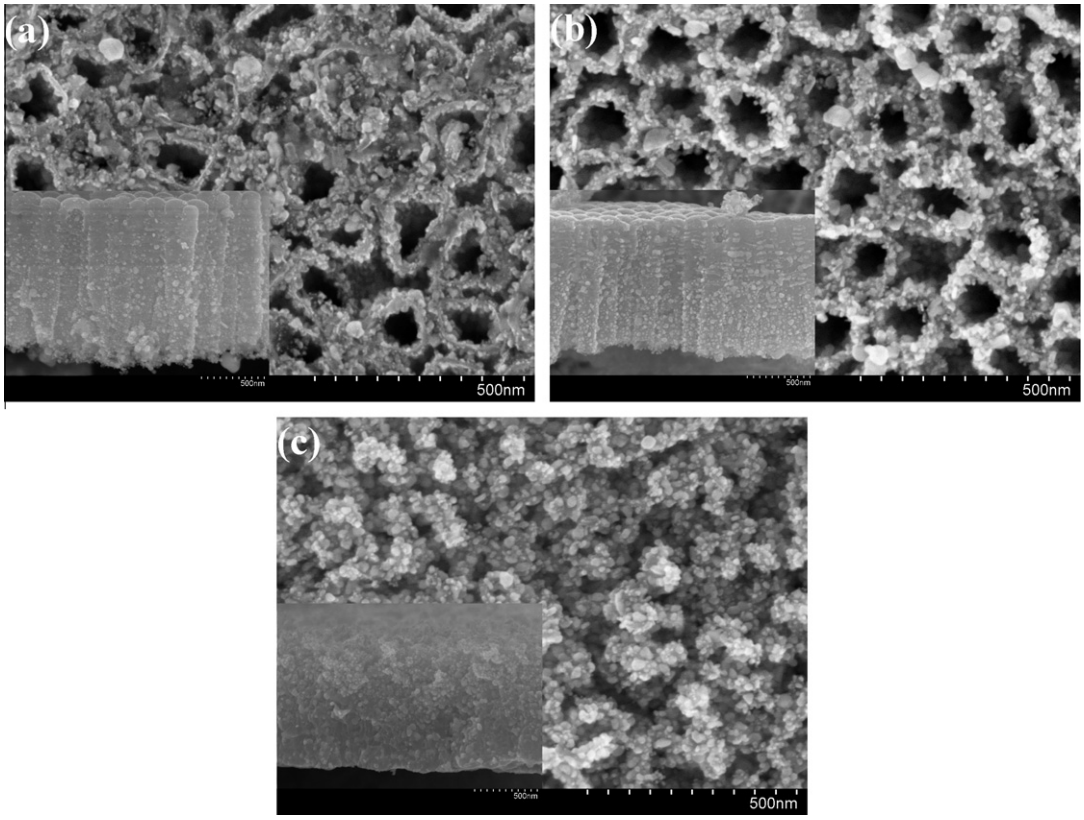

Fig. 2. SEM top images of Ag doped fresh TiO_2 nanotubes by different deposition times, (a) 3 h, (b) 7 h and (c) 11 h (the insets shows the cross-sectional images of the corresponding samples).

In order to investigate the formation process of Ag nanoparticles, the SEM images of Ag doped fresh TiO_2 nanotubes under different deposition times are shown in Fig. 2. In the initial period (3 h), the nucleation of Ag metal takes place. But the Ag metal is not completely evolved, with masses of the agglomerates on the top of the tubes. Afterward (7 h), the Ag nuclei formed in the initial stage provide sufficient new nucleation locations, giving rise to growth of the Ag metal particles (~20 nm). After 11 h, the nanotube structures almost disappear and the as-formed nanosized Ag grains begin to interconnect with each other, along with an enlargement in average diameter to ~27 nm. The nanocrystal agglomeration accelerates the growth of crystal nuclei during this time. The insets in Fig. 2 show the cross-sectional images of the corresponding samples. It can be seen that the distribution of Ag nanoparticles on the tubewalls increases with the deposition time, while the tube length decreases. After depositing for 11 h, the tube structure disappears gradually and only a large amount of Ag particles can be observed in the SEM image.

The samples were further characterized by XRD. Fig. 3I shows the XRD patterns for the different samples in Fig. 1. For the as-prepared TiO_2 thin film (Fig. 3I-a), the nanotubular layer has an amorphous structure. After the deposition of Ag nanoparticles, the five diffraction peaks situated at 38.2, 44.38, 64.66, 77.56, and 40.67° are observed, which are due to the Ag (1 1 1), (2 0 0), (2 2 0), (3 1 1) and Ti (1 0 1) lattice planes, respectively. To address the possible effects of the crystal structure on the performance of the metal oxide as a catalyst support material, some samples of TiO_2 nanotubes were annealed at 723 and 923 K for 1 h in air before the immobilization of Ag nanoparticles. Fig. 3I-b shows the XRD pattern of Ag—TiO_2/723 K. Two diffraction peaks at 25.6° and 48.0° correspond to the facets of anatase TiO_2 (1 0 1) and (2 0 0). Moreover, a weak peak located at 27.86° can be observed, which is ascribed to rutile TiO_2 (1 1 0). This result indicates that the amorphous structure of TiO_2 nanotubes can be transformed to anatase TiO_2 and little amount of rutile TiO_2 after annealing at 723 K. Fig. 3I-c shows the XRD result of Ag—TiO_2/923 K. Compared with the pattern in curve b, another peak appears at 54.35°, which is attributed to rutile TiO_2 (2 1 1). These results confirm the transformation of the anatase TiO_2 to rutile without any significant change of Ag peaks after annealing at 923 K. As shown in Fig. 1c and d, the Ag nanoparticles could be easily deposited on the surface of the TiO_2 tubes annealed at 723 K. Therefore, it can be deduced that the higher crystallinity of the anatase phase plays an important role in improving the bonding strength between Ag and TiO_2. It is worth noting that the relative intensity of the (2 0 0) to (1 1 1) diffraction peaks in Fig. 3I-a, b, and c (0.42, 0.33, and 0.33) was lower than the conventional value (0.46). Here, only (1 1 1) and (2 0 0) peaks were used in the calculation since the intensities of other Ag ($h\,k\,l$) were much lower. This result indicated that the synthesized silver nanoparticles in our system were highly preferred (1 1 1) orientation, because deposited Ag atoms have enough energy to move and the (1 1 1) plane has the lowest free surface energy [21].

Fig. 3II shows the XRD spectra of the Ag doped fresh TiO_2 coating after different deposition times (3, 7, and 11 h). The diffraction peaks in Fig. 3II-a shows the coexistence of Ag and Ti. As shown in the cross-sectional images in Fig. 2, the distribution of Ag nanoparticles on the tubewalls increases and the tube structure disappears with the deposition time. Therefore, the relative intensity of the Ag peaks increase while the Ti peaks become weak in Fig. 3II-b and disappear in Fig. 3II-c. Moreover, the Ag peaks gradually become narrower with an obvious increase in the peak height, indicating high crystallinity of the Ag crystals, in good agreement with the SEM results described previously (Fig. 2).

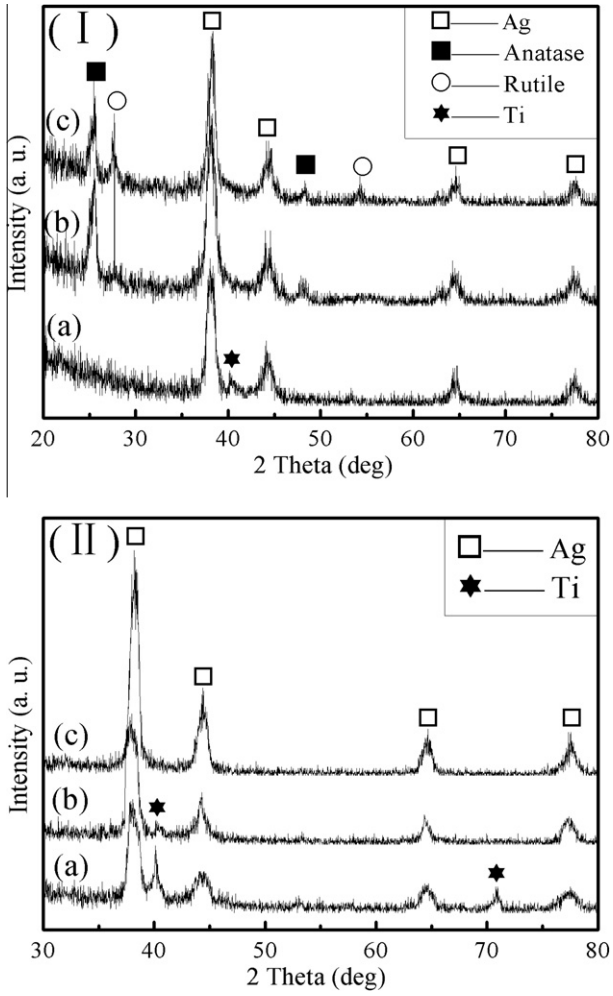

Fig. 3. XRD patterns for Ag—TiO_2 nanotube coatings (I-a), Ag—TiO_2/723 K coatings (I-b), Ag—TiO_2/923 K coatings (I-c), corresponding to the samples in Fig. 1. XRD patterns for Ag—TiO_2/3 h (II-a), Ag—TiO_2/7 h (II-b), Ag—TiO_2/11 h (II-c), corresponding to the samples in Fig. 2.

TEM analyses give further and direct evidence of the existence of Ag nanoparticles on TiO_2 nanostructures with respect to various heat treatments. Fig. 4 depicts the TEM images for the Ag-fresh TiO_2 (I), Ag—TiO_2/723 K coatings (II), and Ag—TiO_2/923 K coatings (III). Fig. 4I and II shows that all samples have similar mean particle sizes. Fig. 4I shows that the Ag nanoparticles are mainly dispersed on the tube wall and bottom. In addition, Ag agglomerates can also be observed in Fig. 4I, which should be attributed to the rapid overgrowth of Ag nanoparticles on the original TiO_2 nanotubes [22]. The high-resolution TEM (HRTEM) images of single particle, located in different areas, are shown in Fig. 4I-a and I-b, where clear lattice fringes can be observed. The amorphous TiO_2 could also be seen clearly. The interplanar spacings of 0.235 and 0.204 nm of crystal lattices are fairly close to those of the (1 1 1) and (2 0 0) plane of Ag. The selected area electron diffraction (SAED) pattern (inset in Fig. 4I) agrees well with the results of the XRD analysis, which indicates that the Ag nanoparticle is of a single, chemically ordered phase rather than a simple mixture of monometallic nanoparticles. Fig. 4II shows the TEM images of the deposited Ag nanoparticles on the TiO_2 nanotubes annealed at 723 K. The nanoparticles are almost uniformly distributed across the surface of each nanotube without aggregation, which are revealed by the lattice fringes of the Ag (1 1 1) plane (0.235 nm) in the HRTEM images shown in Fig. 4II-a and II-b. Also, the structure of the TiO_2 nanotubes is clearly identified as the anatase (1 0 1) plane (0.35 nm) in Fig. 4II-a, which is further confirmed by the SAED pattern shown in the inset of Fig. 4II. It is worth noting that two grains were observed in Fig. 4II-b, as indicated by the black circles. The upper one was identified as $Ag_2Ti_4O_9$, and the lower one as Ag_2TiO_3. There are only two compounds known in the Ag/Ti/O system. One is $Ag_2Ti_4O_9$, which is isostructural to thallium titanate. The other is Ag_2TiO_3 with a novel polymeric titanate anion: TiO_6 octahedra are connected by common edges to form one-dimensionally extended chains [23]. It is well known that the crystal structure of TiO_2 is TiO_6 octahedra. The crystal structure of Ag_2TiO_3 exhibits a novel polymeric metatitanate anion, which consists of distorted TiO_6 octahedra. It means that the Ag_2TiO_3 still retain the original form of the TiO_6 octahedra. Hence, the Ag atoms may react with the TiO_2 to form the Ag_2TiO_3. The reaction mechanism was still not so clear up to date. Each TiO_6 octahedron in Ag_2TiO_3 shares one vertice and four edges with neighboring ones (the structure is similar with that of the ruitle TiO_2). In this study, a small quantity of ruitle TiO_2 was also detected except for the anatase TiO_2 in Ag—TiO_2/723 K coating in Fig. 3I-b. Therefore, it can be inferred that Ag atoms may react with the small amount of ruitle TiO_2 to form the Ag_2TiO_3. The formation mechanism of the other silver titanate $Ag_2Ti_4O_9$ need to be further studied. These silver titanates were not observed in Ag—TiO_2/923 K coating since the poor adhesion between the Ag nanoparticles and TiO_2 nanotubes. However, the two compounds were not detected by XRD, because of the tiny samples used. The HRTEM images (Fig. 4III) of Ag—TiO_2/923 K coating demonstrate that the Ag particles penetrated into the nanotubes, but the tube structure was destroyed because of the high-temperature annealing. Fig. 4III-a and III-b shows the marked (by parallel lines) interplanar spacings of 0.235 and 0.204 nm corresponding to those of the (1 1 1) and (2 0 0) lattice planes of Ag. The corresponding HRTEM image of the TiO_2 substrate indicates that the spacings of the adjacent fringes of the bristles are 0.352 and 0.324 nm, corresponding to the spacings of the (1 0 1) and (1 1 0) planes of the anatase and rutile TiO_2, respectively [24]. This result reconfirms that the anatase TiO_2 can be transformed to the rutile form by annealing at 923 K.

XPS was used to determine the surface compositions of the Ag doped TiO_2 nanotubes. Fig. 5 shows the O 1s, N 1s, Ag 3d, and Ti 2p XPS spectra for the Ag doped fresh TiO_2 nanotubes, and Ag doped nanotubes annealed at 723 and 923 K. Fig. 5a–c are the high-resolution XPS spectra of O 1s for the Ag—TiO_2, Ag—TiO_2/723 K, and Ag—TiO_2/923 K coatings. The spectra exhibit a primary peak at approximately 529.7 and two subpeaks at 531.4 and 532.2 eV in Fig. 5a. The main peak located at 529.9 eV is attributed to titanium dioxide at the surface of the substrate. The peak at 531.4 eV is attributed to correspond to O—H groups, and the peak at 532.2 eV can be attributed to physisorbed water [25]. It can be seen from Fig. 5c that the peak located at 533.2 eV disappeared, but a peak appeared at 532.2 eV for nanotubes annealed at 723 and 923 K. This may result from the incorporation of C—O bonds of EG on the TiO_2 coatings. Fig. 5d shows the N 1s XPS spectra for the three coatings mentioned above. The N 1s peak of the Ag—TiO_2/923 K coating was at 399.5 eV, suggesting the presence of amino groups [26], probably coming from the PVP that did not completely decompose. However, the position of the N 1s peak shifted a little to lower binding energies (399.2 eV) in the Ag-fresh TiO_2 and Ag—TiO_2/723 K coatings, which may be ascribed to the increase of Ag^0 state obtained from the reduction of Ag^+ in $AgNO_3$. This result also confirms that the TiO_2 nanotubes annealed at 923 K are unfavorable for doping Ag nanoparticles, in good agreement with the SEM results. Fig. 5e shows the Ag 3d spectra of the three Ag doped titanium oxide coatings. The binding energy of the Ag 3d5/2 electrons in Ag-fresh TiO_2 and Ag—TiO_2/723 K coatings is 368.2 eV. The above information suggested that Ag existed in the

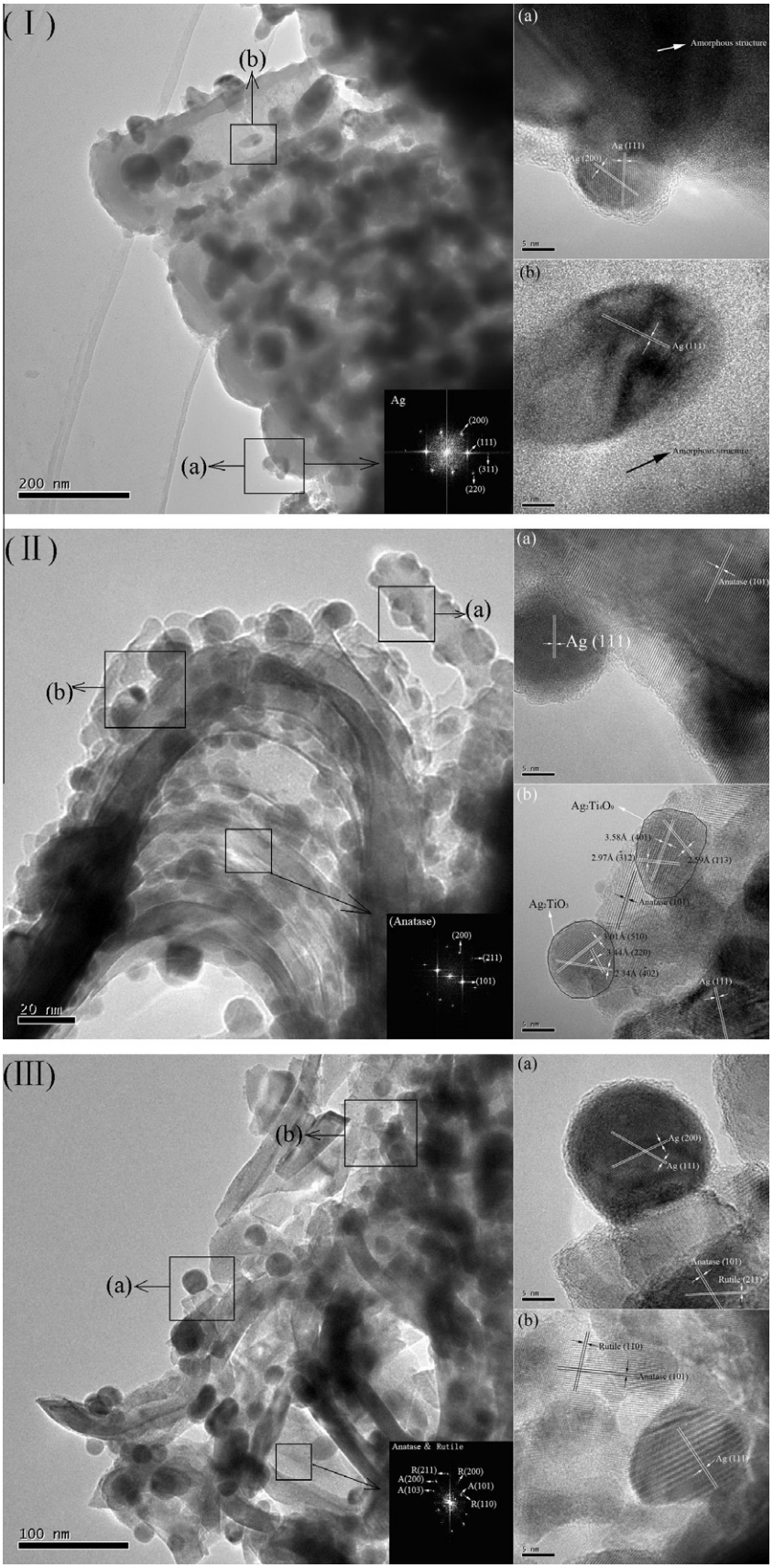

Fig. 4. TEM micrographs for the Ag doped fresh TiO_2 nanotubes (I), Ag doped TiO_2 nanotubes annealed at 723 K (II), Ag doped TiO_2 nanotubes annealed at 923 K (III). The inset shows the electron diffraction pattern corresponding to the square frame.

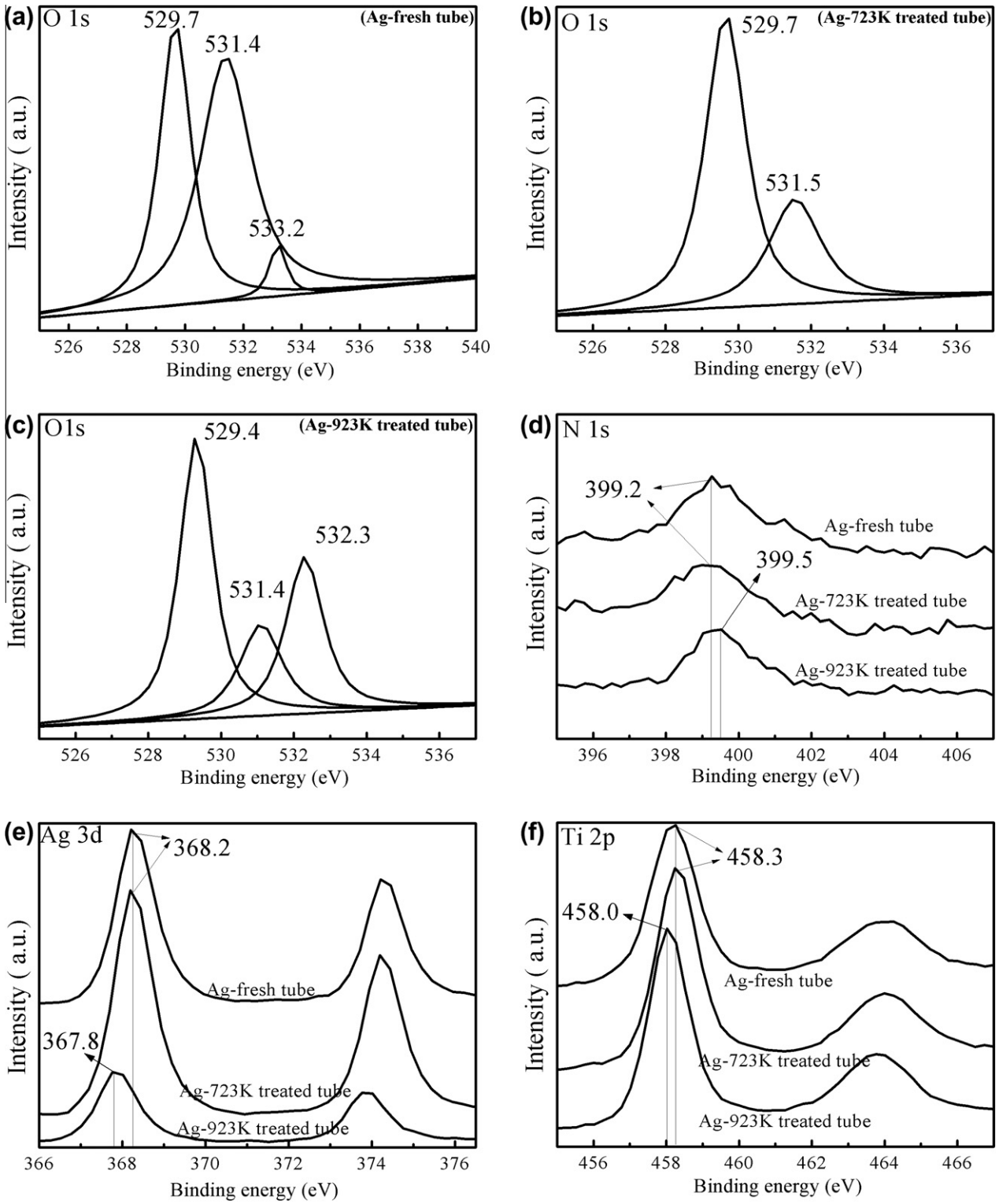

Fig. 5. XPS spectra of (a–c) O 1s, (d) N1s, (e) Ag 3d, and (f) Ti 2p core levels for Ag doped fresh TiO_2 nanotubes, Ag doped TiO_2 nanotubes annealed at 723 K and Ag doped TiO_2 nanotubes annealed at 923 K.

metallic state in the two coatings. As it is known, there are three states of Ag: the Ag^0 state with bonding energy of 368.2 eV, the Ag_2O state with bonding energy of 367.7 eV, and the AgO state with energy of 367.0 eV [27,28]. The Ag 3d5/2 peak of the Ag—TiO_2/923 K coating is located at 367.8 eV. Therefore, it is clear that both Ag^0 and Ag^+ exist in this coating. That is, Ag^+ may exist in two forms in the residual $AgNO_3$ state or the Ag_2O state. The existence of Ag^+ in the $AgNO_3$ state indicates that $AgNO_3$ was not completely reduced. This result is consistent with the N 1s XPS results. The existence of Ag^+ in the Ag_2O state is attributed to the oxidization of Ag^0 particles by the reverse spillover of oxygen-ions from the TiO_2 nanotube crystallites [29]. Fig. 5f shows a representative spectrum of Ti 2p of the three coatings. The binding energy of Ti 2p3/2 is observed at approximately 458.3 eV for the Ag-fresh

TiO_2 and Ag—TiO_2/723 K coatings, which is assigned to the Ti^{4+} [25]. It is known that the two peaks at 457.4 and 458.3 eV match the trivalent and tetravalent states of Ti. Because the binding energy (458 eV) of the Ag—TiO_2/923 K coating is located between the two peaks, both Ti^{3+} and Ti^{4+} exist in this coating. The formation of Ti^{3+} could be the result of the oxidation of CO with molecular oxygen taking place only when the TiO_2 surface was preannealed to above 900 K to produce vacancy sites (Ti^{3+} sites) [30]. Therefore, the presence of Ti^{3+} in the Ag—TiO_2/923 K coating is the result of the TiO_2 surface reaction at the high temperature of 923 K.

To probe the chemical interactions between PVP molecules and $AgNO_3$, the FTIR spectra of the pure PVP, pure $AgNO_3$, and the as-prepared Ag doped TiO_2 nanotubes were obtained at room temperature in the region 4000–400 cm^{-1} (Fig. 6I). To facilitate comparison, the magnified IR spectra of pure PVP and Ag—TiO_2 nanotubes are given, as seen in Fig. 6I-a. It is obvious that the IR spectrum of the Ag—TiO_2 nanotubes is similar to that of pure PVP, indicating the existence of PVP on the Ag—TiO_2 nanostructures. For pure PVP, the bands at 2955, 2924, and 1662 cm^{-1} are usually thought to originate from C—H stretching, asymmetric CH_2 stretching and C=O stretching vibrations (amide I) of the pyrrolidone ring in PVP molecules [31]. In the case of the Ag—TiO_2 nanostructures, the three bands are found to shift to lower wavenumbers compared with those of pure PVP (2917, 2855 and 1644 cm^{-1}). The red-shift of the peaks should be due to the chemical interaction between the PVP molecules and the Ag—TiO_2 surface [32], which was treated with EG saturated with $AgNO_3$ [33]. This band displacement indicates the coordination of amide carbonyl oxygen with Ag species [34]. Besides, the Ag atoms on the surface of the nanotubes may be coordinated with the oxygen atoms of the carbonyl in PVP molecules [31]. The strong vibration associated with the NO_3^- group is located at about 829 and 1397 cm^{-1}, as shown in Fig. 6I-b. The band at 1384 cm^{-1} still exists in the Ag—TiO_2 spectrum, which indicates the presence of $AgNO_3$ in the Ag—TiO_2 nanostructures. However, the vibrational peak at 1397 cm^{-1} became much weaker and the one at 829 cm^{-1} disappeared compared with those of the pure $AgNO_3$, suggesting that the interaction of the NO_3^- related groups with PVP had been weakened for Ag—TiO_2 nanostructures. That is, the formation of the Ag nanostructures doped on the nanotubes was almost completed at this stage [35]. For the FTIR spectrum of pure PVP, other absorption bands positioned between 890 and 1155 cm^{-1} in Fig. 6I-a can be ascribed to the vibration of C—O stretching (1096 cm^{-1}), amide I (C—N) (1074 cm^{-1}), out-of-plane rings C—H bending (1017 and 962 cm^{-1}), respectively [36,37]. It can be seen that these absorption bands are weaker than those of pure PVP. Simultaneously, the peaks at 1287 (—C≡N) and 1440 cm^{-1} (O—H) disappeared. These results indicate that the (—C≡N) in PVP and (CH_2—OH) in EG had been partially decomposed after reaction and the Ag nanoparticles were embedded in the TiO_2 nanotubes by coordination through the O atoms of PVP [34,35,38].

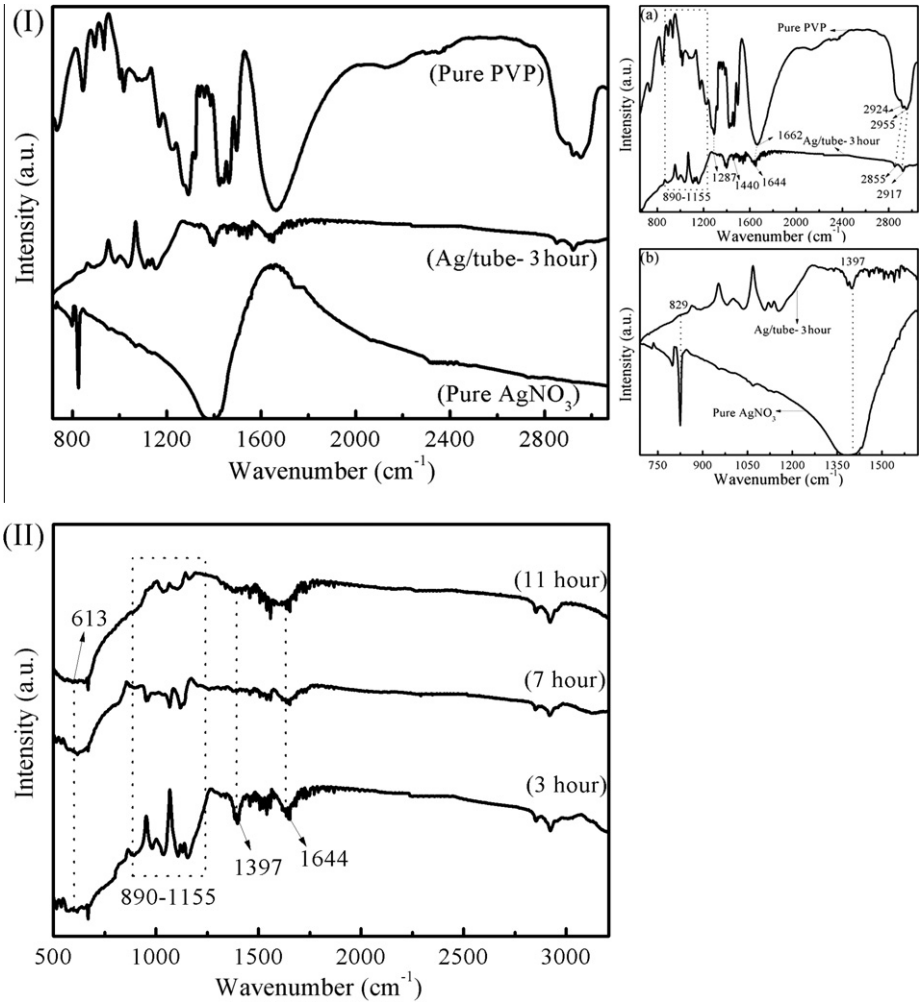

Fig. 6. FTIR spectra of: (I) pure PVP, Ag doped fresh TiO_2 nanotubes for 3 h, pure $AgNO_3$, (a) represents the enlargement of the former two curves, (b) represents the enlargement of the later two curves; (II) Ag doped fresh TiO_2 nanotubes for 3 h, 7 h, 11 h.

To further track the composition evolution during the reaction process, IR spectra of the Ag nanoparticles doped on the TiO_2 nanotubes for different deposition times (3, 7 and 11 h) were performed (see Fig. 6II). The absorption band at about 613 cm^{-1} is assigned to the Ti—O vibration, which is in good agreement with the XRD results [39]. The intensities of the bands between 890 and 1155 cm^{-1} as well as the one at 1644 cm^{-1} became dramatically weaker with deposition time, implying a lower content of organics in the PVP composite. Moreover, the absorption band at 1397 cm^{-1} (NO_3^-) at 7 and 11 h disappears compared with that at 3 h, which indicates that the Ag^+ ions have been completely reduced to Ag nanoparticles at 7 h.

Based on the results of XPS and FTIR, the reactions during the deposition process can be deduced to be as follows. The EG ($HOCH_2CH_2OH$) is a nonelectrolyte with polar groups, such as C—O, C—H, and H—O, which can be absorbed onto TiO_2 by hydrogen bonding [40]. In addition, $NaBH_4$, as a strong reducing agent, can provide H^- ions to reduce Ag^+ ions to Ag^0 atoms directly. The PVP could not only act as a stabilizer to avoid the aggregation of Ag nanoparticles but also participate in the reduction of Ag^+ ions (as confirmed by FTIR and XPS) although the reduction mechanism is still not clear at present. In the presence of $AgNO_3$, some Ag^+ ions were bonded to the polar side groups such as C—O, C—H, and H—O in EG according to Eq. (1) [19], and others were reduced by the H^- supported by $NaBH_4$ based on Eq. (2). Hence, the reduction of Ag^+ ions on the surface of TiO_2 in the EG/$NaBH_4$ solution can occur easily. Both PVP and EG are supposed to repress agglomeration of Ag nanoparticles. In this manner, the Ag nanoparticles can be obtained on the TiO_2 nanotubes.

$$Ag^+ + HO{-}CH_2CH_2{-}OH \rightarrow Ag^0 + HO{-}CH_2CHO + 2H^+ \quad (1)$$

$$Ag^+ + OH^- + H^- \rightarrow Ag^0 + H_2O \quad (2)$$

In order to address the possible effects of the crystal structure of the metal oxide (supported as a catalyst) on the catalytic performance of ethanol, the electrocatalytic performance of the amorphous, anatase, and rutile TiO_2 doped with Ag nanoparticles was investigated in acidic and alkaline media. Fig. 7I shows cyclic voltammetric curves for TiO_2 nanotubes (a), Ag-fresh TiO_2 (b), Ag—TiO_2/723 K coating (c), and Ag—TiO_2/923 K coating (d) in acidic electrolyte solution containing C_2H_5OH (0.5 M)—H_2SO_4 (0.1 M) at a scan rate of 50 mV/s. The hysteresis of (a), (b) and (d) shown as insets in Fig. 7I indicates a nonreversible behavior of the interface in the anodic and cathodic sweeps. This behavior was mainly ascribed to the irreversible doping–dedoping process of the counter anion (SO_4^{2-} or HSO_4^-) in films [41]. However, the Ag—TiO_2/723 K coating under the same electro-experimental conditions has a pair of redox peaks, namely, the oxidation peaks at 0.014 and 0.48 V and the reduction peak at 0.25 V (Fig. 7I-c). In acidic media, the reaction in the electro-oxidation of ethanol has been suggested to follow the series of steps as follows [42,43]:

$$Ag + OH^- = Ag{-}(OH)_{ads} + e^- \quad (3)$$

$$TiO_2 + OH^- = TiO_2{-}(OH)_{ads} + e^- \quad (4)$$

$$Ag + C_2H_5OH = Ag{-}(C_2H_5OH)_{ads} \quad (5)$$

$$Ag{-}(C_2H_5OH)_{ads} + 3OH^- = Ag{-}(CH_3CO)_{ads} + 3H_2O + 3e^- \quad (6)$$

$$Ag{-}(CH_3CO)_{ads} + Ag{-}(OH)_{ads} = Ag{-}CH_3COOH + Ag \quad (7)$$

$$Ag{-}(CH_3CO)_{ads} + TiO_2{-}(OH)_{ads} = Ag{-}CH_3COOH + Ag + TiO_2 \quad (8)$$

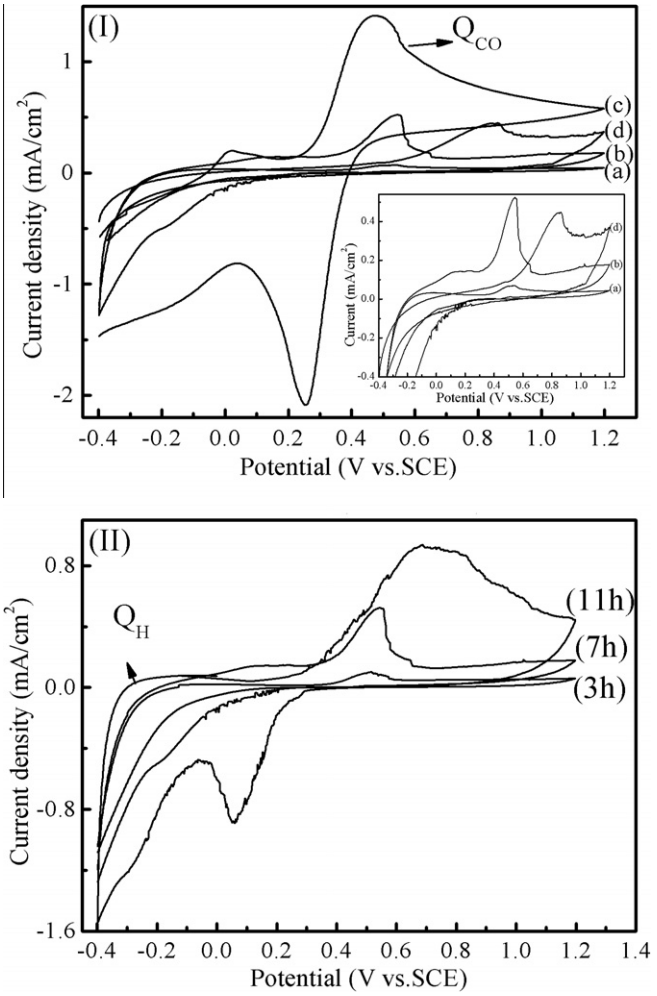

Fig. 7. (I) Cyclic voltammograms in 0.5 M C_2H_5OH and 0.1 M H_2SO_4: (a) pure TiO_2 nanotubes, (b) Ag-fresh TiO_2 nanotubes, (c) Ag—TiO_2 nanotubes annealed at 723 K and (d) Ag—TiO_2 nanotubes annealed at 923 K; (II) Ag-fresh TiO_2 nanotubes for different deposition times (a) 3 h, (b) 7 h, (c) 11 h. Scan rate: 50 mV/s.

The dissociative adsorption of water molecules on the Ag nanoparticles and TiO_2 nanotubes creates the Ag—$(OH)_{ads}$ and TiO_2—$(OH)_{ads}$ surface groups in the first step (Eqs. (3) and (4)). The steps of Eqs. (5) and (6) involve the dehydrogenation process of the C_2H_5OH at the Ag surface, leading to the formation of the poisonous CO-containing intermediates (—CH_3CO) deposited on the active sites of the Ag [44]. To continue the catalytic oxidation reaction, the Ag—$(OH)_{ads}$ and TiO_2—$(OH)_{ads}$ groups adjacent to the Ag nanoparticles may readily oxidize the CO-containing groups bonded to the peripheral Ag atoms, and the adsorbed CO-containing intermediates are removed from the surface to regenerate the active Ag sites (Eqs. (6) and (7)). That is, the weak plateau (O1) at 0.014 V was attributed to the direct oxidation of ethanol ($CH_3CH_2OH{=}CH_3CH_2O^-{=}H^+$) via a dehydrogenation pathway. Here, "CH_3CH_2O" is the dehydrogenation intermediate [45]. The second large anodic peak (O2) at 0.48 V was related to the formation of $(-CH_3CO)_{ads}$, which results from the dehydration of ethanol [46].

It is clearly seen that the peak current density for the oxidation of ethanol is in the following order: 0.064 (for TiO_2 nanotubes) (a) <0.44 (for Ag—TiO_2/923 K coating) (d) <1.08 (for Ag-fresh TiO_2 coating) (b) <1.44 mA/cm^2 (for Ag—TiO_2/723 K coating) (c). The peak current density results confirm the efficiency of crucial Ag nanoparticles toward the catalytic oxidation of ethanol. The Ag nanoparticles can improve the adsorption of ethanol on the

catalytic sites, and the anodic current for the oxidation of ethanol is ultimately increased. Another noticeable feature is that for the Ag—TiO_2/723 K electrode, the onset potential for ethanol oxidation is much lower than those for the other three electrodes. It is known that the onset potential is related to the breaking of C—H bonds and the subsequent removal of intermediates by oxidation with $(OH)_{ads}$ [47,48]. A lower onset potential indicates that the overpotential for ethanol oxidation is lower and that electrocatalytic ethanol oxidation occurs more easily on the electrode [49]. In order to gain insight into the effect of deposition time on the electrochemical properties, the cyclic voltammograms of the Ag-fresh TiO_2 coating at deposition times of 3, 7, and 11 h are also presented. It can be seen that there is a strong oxidation peak at 0.7 and a reduction peak at 0.058 V in the Ag-fresh TiO_2-11 h coating. However, the Ag-fresh TiO_2-3 h and Ag-fresh TiO_2-7 h coatings have only an irreversible oxidation peak at 0.52 and 0.55 V (Fig. 7II). All samples exhibit features of the hydrogen adsorption/desorption region between −0.4 and 0.28 V (vs SCE), and the oxide formation/desorption regions are observed at potentials of 0.45, 0.455, and 0.71 V for the Ag-fresh TiO_2-3 h, Ag-fresh TiO_2-7 h, and Ag-fresh TiO_2-11 h catalysts, respectively. It is known that the integrated intensity of hydrogen desorption represents the number of active sites of Ag nanoparticles. The coulombic charges for hydrogen desorption (Q_H) on the Ag-fresh TiO_2-3 h, Ag-fresh TiO_2-7 h, and Ag-fresh TiO_2-11 h catalysts were 1.46, 3.74, and 5.78 mC cm^{-2}, respectively. The electrochemical active surface area (EASA) is calculated according to the formula EASA = $Q_H/(Q_{ref1}\cdot[Ag])$, where [Ag] is the Ag loading in the electrode ([Ag] = 0.027, 0.048 and 0.056 mg/cm^2). Q_{ref1} is a constant that represents the charge required to oxidize a monolayer of H_2 on bright Ag. The calculated EASA of the Ag-fresh TiO_2-11 h catalyst is higher than the corresponding values for the Ag-fresh TiO_2-7 h and Ag-fresh TiO_2-3 h catalysts, which means that the former has a larger EASA than the later two. The higher EASA appears to be due to the increased surface area of the Ag nanoparticles when exposed to the ethanol solution. Therefore, a longer deposition time results in an increased density of the active sites on the electrode surface.

Fig. 8I shows the typical cyclic voltammograms of the same coatings in Fig. 7I in alkaline media (0.5 M C_2H_5OH and 0.1 M NaOH). Similar phenomena can be observed in Fig. 8I as in Fig. 7I. However, compared with Fig. 7I, all the coatings show obvious oxidation and reduction peaks except the TiO_2 nanotube coating. The lower electrocatalytic activity of TiO_2 nanotube coating in alkaline media may be the result of slower charge transfer [50]. Besides, the peak current density for the Ag—TiO_2/723 K coating increases significantly. The coulombic charge $Q_{(—CH3CO)ads}$ is related to the electro-oxidation of the adsorbed CO-containing intermediates in the reactions of (3) and (7). $Q_{(—CH3CO)ads}$ was used to compare the active surface of the catalysts [51]. [Ag] represents the Ag loading in the electrode. $EASA_{(—CH3CO)ads}$ can also be calculated by the equation of $EASA_{(—CH3CO)ads} = Q_{(—CH3CO)ads}/(Q_{ref2}\cdot[Ag])$, where Q_{ref2} is the charge density required to oxidize a monolayer of CO-containing intermediates on bright Ag. The values of the charge $Q_{(—CH3CO)ads}$ for the Ag—TiO_2/723 K coating in acidic and alkaline media are 0.54 and 1.02 mC cm^{-2}, respectively, and the product $Q_{ref2}\cdot[Ag]$ is a constant value. The calculation so obtained shows that the active surface in alkaline media is larger than that in acidic media, which indicates a higher catalytic activity in alkaline media [1]. In addition, in the forward scan, the peak at about 0.35 V (versus SCE) is smaller than the potential of 0.45 V in acidic media, which indicates that the electrocatalytic ethanol oxidation in alkaline media occurs more easily than that in acidic media by use of Ag—TiO_2/723 K coating as a catalyst. The steps for the oxidation and reduction of ethanol are as follows. Initially, the reaction sites are covered by a layer of adsorbed CO-containing intermediates generated from ethanol dehydrogenation. Some of the weakly adsorbed CO-containing intermediates begin to be oxidized with the increasing potential. Then, ethanol oxidation takes place. Subsequently, the backward scan will provoke reduction process [50].

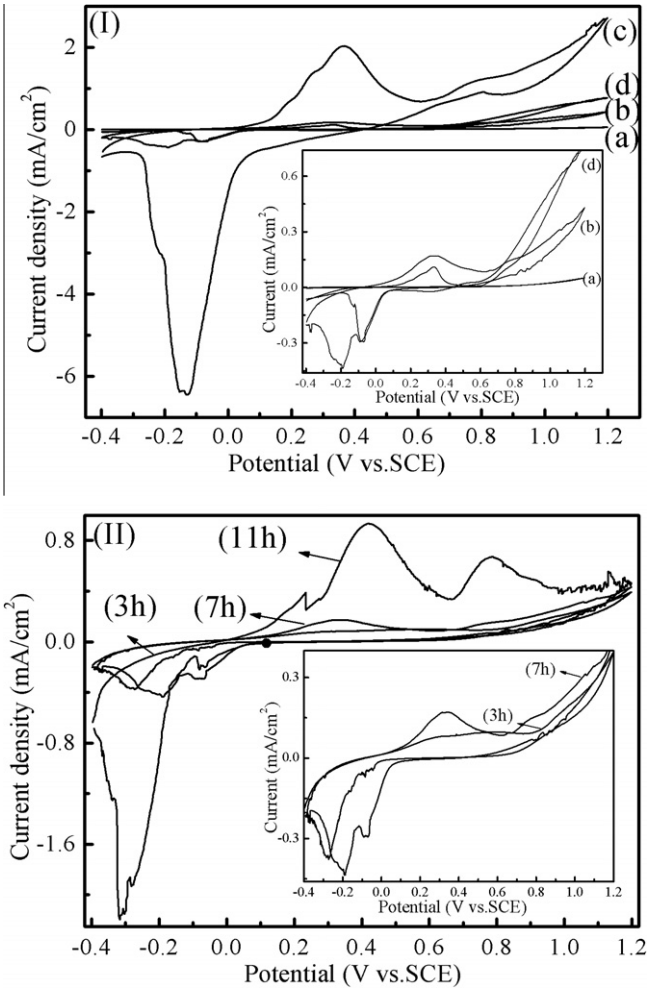

Fig. 8. (I) Cyclic voltammograms in 0.5 M C_2H_5OH and 0.1 M NaOH: (a) pure TiO_2 nanotubes, (b) Ag-fresh TiO_2 nanotubes, (c) Ag—TiO_2 nanotubes annealed at 723 K and (d) Ag—TiO_2 nanotubes annealed at 923 K; (II): Ag-fresh TiO_2 nanotubes for different deposition times (a) 3 h, (b) 7 h, (c) 11 h. Scan rate: 50 mV/s.

For better understanding of the above described synergistic effect of the Ag nanoparticles and the TiO_2/723 K support, Fig. 9 schematically illustrates the likely reaction steps of the oxidation of CO-containing intermediates on the Ag nanoparticle, which can also be described by the reactions of Eqs. (3)–(8) mentioned above. Fig. 9a shows the reactions of Eqs. (3), (5), (6), and (7) and Fig. 9b shows the reactions of Eqs. (4), (5), (6), and (8).

The Ag—$(CH_3CO)_{ads}$ groups were formed by ethanol oxidation (Eqs. (5) and (6)). Because alkaline media can provide sufficient OH^- to form abundant TiO_2—$(OH)_{ads}$ groups with anatase TiO_2, a reaction between TiO_2—$(OH)_{ads}$ and Ag—$(CH_3CO)_{ads}$ occurred, giving rise to Ag—CH_3COOH and enhancing both the current density and the poison resistance. Fig. 8II shows the cyclic voltammograms of the same coatings in Fig. 7II in alkaline media (0.5 M C_2H_5OH and 0.1 M NaOH). It can be seen that the Ag-fresh TiO_2-11 h coatings show two oxidation peaks related to the oxidation of ethanol and the corresponding intermediates produced during the ethanol oxidation [52]. Besides, both the oxidation and reduction peaks are observed in Fig. 8II, indicating the redox of the Ag-fresh TiO_2 coatings was reversible in alkaline media. Moreover, the peak currents related to the oxidation of ethanol in alkaline media did not increase greatly for the three coatings when compared to the system

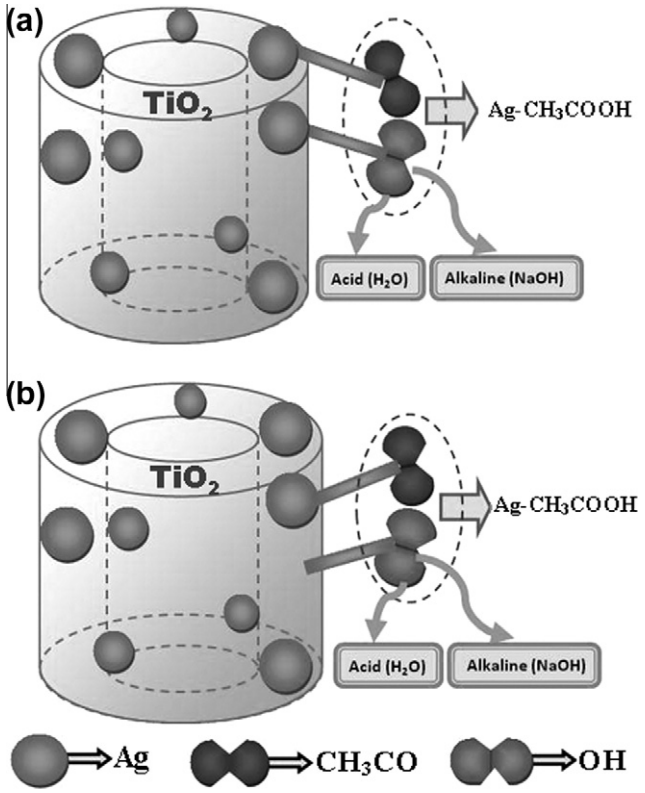

Fig. 9. Schematic diagram of the electrocatalytic mechanism in acidic and alkaline media. (a) The synergistic effect of the Ag nanoparticles on CO-containing intermediates (—CH_3CO) oxidation; (b) the synergistic effect of the Ag nanoparticles and TiO_2 nanotubes on CO-containing intermediates (—CH_3CO) oxidation.

supported in acidic media. However, the EASA shows the same result with Fig. 7II that the longer deposition time results in a higher EASA, which indicates that the Ag-fresh TiO_2/11 h coating has the best electrocatalytic activity in both acidic and alkaline media.

The results obtained mentioned above may indicate that the Ag nanocrystal has been reconstructed during the stability test and the basal plane of Ag (1 1 1) becomes the main plane, as shown in Fig. 4. The more exposed Ag (1 1 1) surface on Ag nanoparticles would lead to higher activity [53]. Furthermore, the Ag—TiO_2/723 K coatings process significantly improved the performance of catalytic activity in both acidic and alkaline media. There are two possible explanations for this observation. The first possibility is relatively weak adherence of Ag nanoparticles onto the nonannealed nanotubular surfaces [54]. The other possibility is that a small amount of silver titanates were obtained by depositing Ag nanoparticles on the TiO_2/723 K nanotubes (as shown in Fig. 4), which indicates that the Ag cannot only be deposited but also be doped in the TiO_2 nanotubes. It is known that crystal structure distortion can contribute to superior catalytic activity [55,56]. Therefore, the TiO_6 distortion of silver titanates may result in the narrow band-gap and increased state density of Ag—TiO_2/723 K coating, facilitating the migration of charge carriers and enhanced catalytic activity [57]. However, the catalytic activity of Ag—TiO_2/923 K was lower than that of Ag—TiO_2/723 K. This result can be attributed to two reasons. On the one hand, the low catalytic activity is most likely caused by less Ag deposition; on the other hand, the Ag_2TiO_3 can not be obtained in the Ag—TiO_2/923 K coating since the poor adhesion between the Ag nanoparticles and TiO_2 nanotubes. What is even more important is that the bottom of the nanotubes was destroyed by annealing at a higher temperature (Fig. 2). Therefore, the irregular structure of the nanotubes might be a negative influence on loading Ag nanoparticles.

4. Conclusions

In the present study, Ag—TiO_2 nanotube catalysts with high activity are successfully synthesized by a simple reduction method in an aqueous solution. The results reveal that the Ag nanoparticles are anchored onto TiO_2 nanotubes. It is also found that Ag atoms react with the small amount of ruitle TiO_2 to form the silver titanates. The cyclic voltammetry measurements for ethanol oxidation show that Ag—TiO_2/723 K coatings have the best catalytic activity. The excellent performance of this catalyst can be attributed to the following three aspects: (1) the well-dispersed Ag nanoparticles on the surface of TiO_2 nanotubes (Ag simultaneously doped and deposited on TiO_2 nanotubes) result in a higher electrochemical surface area and much better electocatalytic activity; (2) Ag works as the main dehydrogenation site. The more exposed Ag (1 1 1) surface on Ag nanoparticles can lead to higher activity; and (3) the anatase TiO_2 facilitates the removal of the CO-containing intermediates, leading to an enhanced catalytic activity. In summary, the Ag—TiO_2 nanotube coating is a promising catalyst for ethanol electro-oxidation.

Acknowledgment

This work was supported by Key Project in the Science & Technology Pillar Program of Tianjin (09ZCKFGX29100).

References

[1] L.X. Yang, Y. Xiao, G.M. Zeng, S.L. Luo, S.Y. Kuang, Q.Y. Cai, Energy Fuel 23 (2009) 3134.
[2] J. Mann, M.S. Daubin, A.B. Bocarsly, Am. Chem. Soc. Div. Fuel Chem. 49 (2004) 662.
[3] M. Paulose, K. Shankar, S. Yoriya, H.E. Prakasam, O.K. Varghese, G.K. Mor, T.J. LaTempa, A. Fitzgerald, C. Grimes, J. Phys. Chem. B 112 (2008) 15261.
[4] D. Xu, S. Bliznakov, Z.P. Liu, J.Y. Fang, N. Dimitrov, Angew. Chem. Int. Ed. 49 (2009) 1282.
[5] L.F. Liu, E. Pippel, R. Scholz, U. Gosele, Nano Lett. 9 (2009) 4352.
[6] Z.Y. Zhou, Z.Z. Huang, D.J. Chen, Q. Wang, N. Tian, S.G. Sun, Angew. Chem. Int. Ed. 49 (2010) 411.
[7] C.W. Xu, H. Wang, P.K. Shen, S.P. Jiang, Adv. Mater. 19 (2007) 4256.
[8] J. Selva, S.E. Martinez, D. Buceta, M.J. Rodriguez-Vazquez, M.C. Blanco, M.A. Lopez-Quintela, G. Egea, J. Am. Chem. Soc. 132 (2010) 6947.
[9] T. Murakata, Y. Higashi, N. Yasui, T. Higuchi, S. Sato, J. Chem. Eng. Jpn. 35 (2002) 1270.
[10] T. Sreethawong, Y. Suzuki, S. Yoshikawa, C. R. Chim. 9 (2006) 307.
[11] I. Paramasivalm, J.M. Macak, P. Schmuki, Electrochem. Commun. 10 (2008) 71.
[12] J. Joo, S.G. Kwon, T. Yu, M. Cho, J. Lee, J. Yoon, T. Hyeon, J. Phys. Chem. B 109 (2005) 15297.
[13] S. Yoo, S.A. Akbar, K.H. Sandhage, Adv. Mater. 16 (2004) 260.
[14] J. Zhou, Y. Ding, S.Z. Deng, L. Gong, N.S. Xu, Z.L. Wang, Adv. Mater. 17 (2005) 2107.
[15] C.C. Li, K.L. Shuford, Q.H. Park, W.P. Cai, Y. Li, E.J. Lee, S.O. Cho, Angew. Chem. Int. Ed. 46 (2007) 3264.
[16] M. Zhou, S.H. Chen, S.Y. Zhao, H.F. Ma, Chem. Lett. 34 (2005) 1670.
[17] Y.G. Sun, Y.D. Yin, B.T. Mayers, T. Herricks, Y.N. Xia, Chem. Mater. 14 (2002) 4736.
[18] A. Gautam, G.P. Singh, S. Ram, Synth. Met. 157 (2007) 5.
[19] W. Su, S.S. Wei, S.Q. Hu, J.X. Tang, J. Hazard. Mater. 172 (2009) 716.
[20] Y.Q. Liang, X.J. Yang, Z.D. Cui, S.L. Zhu, Curr. Nanosci. 6 (2010) 256.
[21] T. Feng, B.Y. Jiang, S. Zhuo, X. Wang, X.H. Liu, Appl. Surf. Sci. 254 (2008) 1565.
[22] F.X. Zhang, N.J. Guan, Y.Z. Li, X. Zhang, J.X. Chen, H.S. Zeng, Langmuir 19 (2003) 8230.
[23] C. Linke, M. Jansen, J. Solid State Chem. 134 (1997) 17.
[24] J.M. Du, J.L. Zhang, Z.M. Liu, B.X. Han, T. Jiang, Y. Huang, Langmuir 22 (2006) 1307.
[25] F. Zhang, G.K. Wolf, X.H. Wang, X.H. Liu, Surf. Coat. Technol. 148 (2001) 65.
[26] E. Traversa, M.L. Di Vona, P. Nunziante, S. Licoccia, J.W. Yoon, T. Sasaki, N. Koshizaki, J. Sol–Gel Sci. Technol. 22 (2001) 115.
[27] I.M. Arabatzis, T. Stergiopoulos, M.C. Bernard, D. Labou, S.G. Neophytides, P. Falaras, Appl. Catal. B – Environ. 42 (2003) 187.
[28] G.I.N. Waterhouse, G.A. Bowmaker, J.B. Metson, Appl. Surf. Sci. 183 (2001) 191.
[29] J. Nicole, D. Tsiplakides, C. Pliangos, X.E. Verykios, C. Comninellis, C.G. Vayenas, J. Catal. 204 (2001) 23.
[30] A. Linsebigler, C. Rusu, J.T. Yates, J. Am. Chem. Soc. 118 (1996) 5284.
[31] Y. Gao, L. Song, P. Jiang, L.F. Liu, X.Q. Yan, Z.P. Zhou, D.F. Liu, J.X. Wang, H.J. Yuan, Z.X. Zhang, X.W. Zhao, X.Y. Dou, W.Y. Zhou, G. Wang, S.S. Xie, H.Y. Chen, J.Q. Li, J. Cryst. Growth 276 (2005) 606.

[32] N. Sheikh, A. Akhavan, M.Z. Kassaee, Physica E 42 (2009) 132.
[33] X.F. Qian, J. Yin, S. Feng, S.H. Liu, Z.K. Zhu, J. Mater. Chem. 11 (2001) 2504.
[34] A. Slistan-Grijalva, R. Herrera-Urbina, J.F. Rivas-Silva, M. Avalos-Borja, F.F. Castillon-Barraza, A. Posada-Amarillas, Mater. Res. Bull. 43 (2008) 90.
[35] M. Jin, X.T. Zhang, S. Nishimoto, Z.Y. Liu, D.A. Tryk, T. Murakami, A. Fujishima, Nanotechnology 18 (2007) 075605.
[36] E.M. Abdelrazek, I.S. Elashmawi, A. El-Khodary, A. Yassin, Curr. Appl. Phys. 10 (2009) 607.
[37] M.S. Sadjadi, N. Farhadyar, K. Zare, Superlattice Microstruct. 46 (2009) 483.
[38] G.P. Dong, X.D. Xiao, X.F. Liu, B. Qian, Z.J. Ma, S. Ye, D.P. Chen, J.R. Qiu, J. Nanopart. Res. 12 (2010) 1319.
[39] F.L. Toma, G. Bertrand, S. Begin, C. Meunier, O. Barres, D. Klein, C. Coddet, Appl. Catal. B – Environ. 68 (2006) 74.
[40] A. Borras, A. Barranco, F. Yubero, A.R. Gonzalez-Elipe, Nanotechnology 17 (2006) 3518.
[41] W.Q. Zhou, Y.K. Du, H.M. Zhang, J.K. Xu, P. Yang, Electrochim. Acta 55 (2010) 2911.
[42] S.T. Nguyen, H.M. Law, H.T. Nguyen, N. Kristian, S.Y. Wang, S.H. Chan, X. Wang, Appl. Catal. B – Environ. 91 (2009) 507.
[43] Z.X. Liang, T.S. Zhao, J.B. Xu, L.D. Zhu, Electrochim. Acta 54 (2009) 2203.
[44] N.W. Maxakato, K.I. Ozoemena, C.J. Arendse, Electroanalysis 22 (2010) 519.
[45] B. Jorgensen, S.E. Christiansen, M.L.D. Thomsen, C.H. Christensen, J. Catal. 251 (2007) 332.
[46] J.H. Choi, K.J. Jeong, Y. Dong, J. Han, T.H. Lim, J.S. Lee, Y.E. Sung, J. Power Sour. 163 (2006) 71.
[47] S.L. Gojkovic, T.R. Vidakovic, D.R. Durovic, Electrochim. Acta 48 (2003) 3607.
[48] G. Wu, D.Y. Li, C.S. Dai, D.L. Wang, N. Li, Langmuir 24 (2008) 3566.
[49] X. Li, G. Chen, J. Xie, L.J. Zhang, D.G. Xia, Z.Y. Wu, J. Electrochem. Soc. 157 (2010) B580.
[50] Y.Z. Lei, G.H. Zhao, X.L. Tong, M.C. Liu, D.M. Li, R. Geng, Chemphyschem 11 (2010) 276.
[51] A. Pozio, M. De Francesco, A. Cemmi, F. Cardellini, L. Giorgi, J. Power Sour. 105 (2002) 13.
[52] G. Selvarani, S. Maheswari, P. Sridhar, S. Pitchumani, A.K. Shukla, J. Electrochem. Soc. 156 (2009) B1354.
[53] X.M. Liu, M.Y. Li, G.Y. Han, J.H. Dong, Electrochim. Acta 55 (2010) 2983.
[54] J.M. Macak, P.J. Barczuk, H. Tsuchiya, M.Z. Nowakowska, A. Ghicov, M. Chojak, S. Bauer, S. Virtanen, P.J. Kulesza, P. Schmuki, Electrochem. Commun. 7 (2005) 1417.
[55] R. Asahi, T. Morikawa, T. Ohwaki, K. Aoki, Y. Taga, Science 293 (2001) 269.
[56] X.T. Hong, Z.P. Wang, W.M. Cai, F. Lu, J. Zhang, Y.Z. Yang, N. Ma, Y.J. Liu, Chem. Mater. 17 (2005) 1548.
[57] N. Markovic, H. Gasteiger, P.N. Ross, J. Electrochem. Soc. 144 (1997) 1591.